MIMO IMPEDANCE BASED STABILITY ANALYSIS OF DFIG-BASED WIND FARM WITH MMC-HVDC IN MODIFED SEQUENCE DOMAIN

Haoxiang Zong[1], Jing Lyu[1], Chen Zhang[2], Xu Cai[1], Marta Molinas[2], Fangquan Rao[1]*

[1] *Wind Power Research centre of Shanghai Jiao Tong University, Shanghai, China*
[2] *Department of Engineering Cybernetics, Norwegian University of Science and Technology, Trondheim, Norway*
* *xucai@sjtu.edu.cn*

Keywords: MULTI-INOUT-MULTI-OUTPUT, MMC-HVDC, FREQUENCY COUPLING, WIND FARM

Abstract

The modular multilevel converter (MMC) based high-voltage direct current (HVDC) transmission is widely applied for the large-scale wind farm integration making its interaction stability analysis especially significant. However, only a few related researches have so far been done and most of them depict ac-side characteristics of the connected MMC station using simplified single-input-single-output (SISO) impedance, which is not able to reflect all harmonic couplings and sequence couplings. To solve this issue, based on the harmonic state-space method, the multi-input-multi-output (MIMO) impedance model of the MMC in modified sequence domain are established to better characterize the MMC's off-diagonal coupling effects. Also, the accurate MIMO impedance model of the doubly-fed induction generator (DFIG) based wind farm is used in this paper. Subsequently, the generalized Nyquist criterion is applied to analyse the stability of such MIMO interconnected system. The accuracy of the established MMC's MIMO impedance model is verified via the frequency scanning, and the theoretical stability analysis of the interconnected system is validated by time-domain simulations in Matlab/Simulink.

1 Introduction

With the wind power penetration rate continuously rising, the Modular Multilevel Converter (MMC) High Voltage Direct Current (HVDC) transmission schemes [1] is getting more and more attention in recent years. Compared with the Voltage Source Converter (VSC) based HVDC, the MMC-HVDC has some outstanding advantages, such as modularity, reduced converter losses, high efficiency and so on. However, due to the complex internal dynamics of the MMC, the instability phenomenon like oscillation and resonance is extremely prone to happen between the wind farm and the MMC-HVDC [2-4]. Therefore, it's meaningful and urgent to implement the accurate stability analysis of such interconnected system to provide a guide for the power system operators.

In the past research, some simplifications are made to reveal the internal interaction mechanism of the oscillation happened between the wind farm and the MMC-HVDC. The simplified single-input-single-output (SISO) impedance model is usually used to characterize the MMC's ac-side dynamics, and the wind farm model used is also simplified a lot [2-7]. It's reasonable to make these assumptions at the beginning because the interconnected system is so complicated. At present, based on the past research, more accurate models and stability analysis are carried out in this paper. According to the modified domain concept defined in [8], the more accurate multi-input-multi-output (MIMO) sequence impedance model of the MMC is established.

Multiple methods have been proposed to model the ac-side impedance characteristics of the MMC, such as the multi-harmonic linearization method [9], [10] and harmonic state-space method (HSS) [11]. The HSS method is selected in this paper to derive the MIMO impedance model of the MMC due to its advantages, like intuitive and rigorousness [11], [12]. The off-diagonal couplings between positive and negative sequence of the MMC are taken into account in the modified sequence impedance model developed in this paper. Correspondingly, the DFIG-based wind farm is also modelled in modified sequence domain [13]. Under this circumstance, the source and load subsystem are all modelled in the same dimension which can be analysed using the generalized Nyquist criterion.

The rest of the paper is organized as below. In section 2, the small-signal three-phase model of MMC under ac-voltage control is established. In section 3, the modified sequence impedance model of the MMC is derived based on HSS method. In section 4, the DFIG-based wind farm is connected with the MMC-HVDC to implement the stability analysis in modified sequence domain. The correctness of the theoretical analysis is validated in Matlab/Simulink.

2 Small-signal Three-Phase Model of MMC

In this part, the small-signal state-space model of the MMC under ac-voltage control is derived. The challenging part is to transform all control state variables in *d-q* frame to those in *abc* frame. The grid-side MMC is simplified as an ideal dc voltage assuming that the dc dynamics are relatively small. The topology of the studied interconnected system is shown in Fig.1, where the DFIG-based wind farm is modelled based on the aggregation method. The detailed DFIG is considered in this paper which takes the dc-coupling effects into account. The small-signal model of the MMC is derived in the following part.

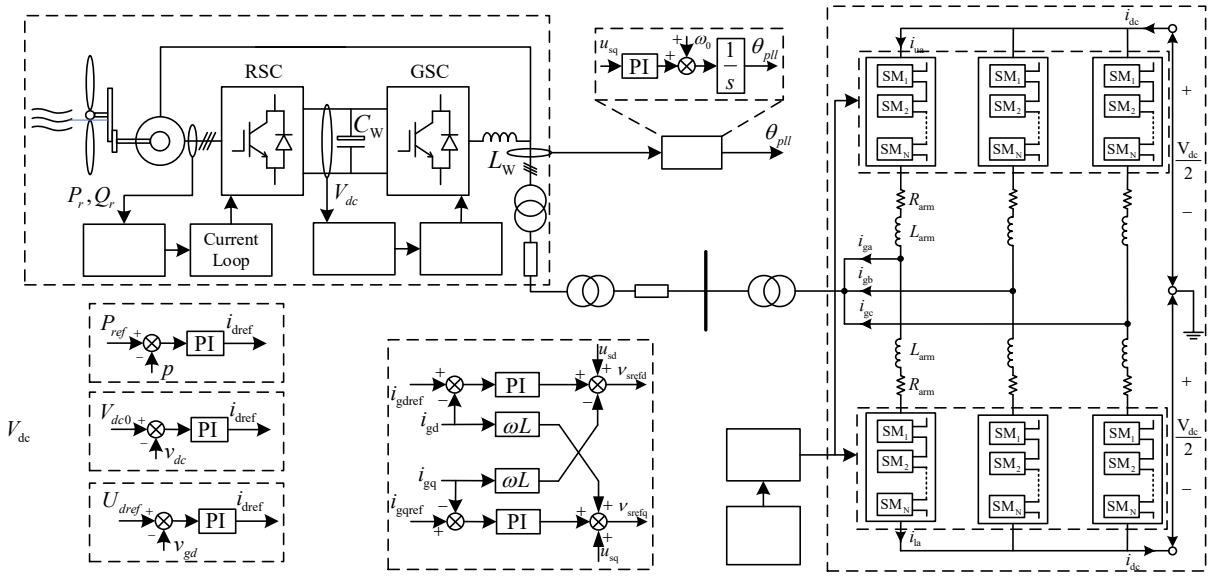

Fig. 1 The topology of the DFIG-based wind farm connected to the MMC-HVDC

2.1 Small-signal three-phase model of the main circuit

Periodic time-varying model of the MMC has been studied well [14] and here the three-phase small-signal model of the main circuit is given in (1) ~ (4).

$$\frac{\mathrm{d}\Delta \boldsymbol{i}_{\mathrm{cx}}}{\mathrm{dt}}=-\frac{R}{L}\Delta \boldsymbol{i}_{\mathrm{cx}}-\frac{\boldsymbol{n}_{\mathrm{uxs}}}{2L}\Delta \boldsymbol{v}_{\mathrm{cux}}-\frac{\boldsymbol{n}_{\mathrm{lxs}}}{2L}\Delta \boldsymbol{v}_{\mathrm{clx}}-\frac{\boldsymbol{v}_{\mathrm{cuxs}}}{2L}\Delta \boldsymbol{n}_{\mathrm{ux}}-\frac{\boldsymbol{v}_{\mathrm{clxs}}}{2L}\Delta \boldsymbol{n}_{\mathrm{lx}} \tag{1}$$

$$\frac{\mathrm{d}\Delta \boldsymbol{v}_{\mathrm{cux}}}{\mathrm{dt}}=\frac{\boldsymbol{n}_{\mathrm{uxs}}}{C_{\mathrm{arm}}}\left(\Delta \boldsymbol{i}_{\mathrm{cx}}+\frac{1}{2}\Delta \boldsymbol{i}_{\mathrm{gx}}\right)+\frac{1}{C_{\mathrm{arm}}}\left(\boldsymbol{i}_{\mathrm{cxs}}+\frac{1}{2}\boldsymbol{i}_{\mathrm{gxs}}\right)\Delta \boldsymbol{n}_{\mathrm{ux}} \tag{2}$$

$$\frac{\mathrm{d}\Delta \boldsymbol{v}_{\mathrm{clx}}}{\mathrm{dt}}=\frac{\boldsymbol{n}_{\mathrm{lxs}}}{C_{\mathrm{arm}}}\left(\Delta \boldsymbol{i}_{\mathrm{cx}}-\frac{1}{2}\Delta \boldsymbol{i}_{\mathrm{gx}}\right)+\frac{1}{C_{\mathrm{arm}}}\left(\boldsymbol{i}_{\mathrm{cxs}}-\frac{1}{2}\boldsymbol{i}_{\mathrm{gxs}}\right)\Delta \boldsymbol{n}_{\mathrm{lx}} \tag{3}$$

$$\frac{\mathrm{d}\Delta \boldsymbol{i}_{\mathrm{gx}}}{\mathrm{dt}}=\frac{\boldsymbol{n}_{\mathrm{lxs}}}{L}\Delta \boldsymbol{v}_{\mathrm{clx}}-\frac{\boldsymbol{n}_{\mathrm{uxs}}}{L}\Delta \boldsymbol{v}_{\mathrm{cux}}+\frac{\boldsymbol{v}_{\mathrm{clxs}}}{L}\Delta \boldsymbol{n}_{\mathrm{lx}}-\frac{\boldsymbol{v}_{\mathrm{cuxs}}}{L}\Delta \boldsymbol{n}_{\mathrm{ux}}-\frac{R+Z_{\mathrm{L}}}{L}\Delta \boldsymbol{i}_{\mathrm{gx}} \tag{4}$$

Where the state variable $\boldsymbol{i}_{\mathrm{cx}}$, $\boldsymbol{v}_{\mathrm{cux}}$, $\boldsymbol{v}_{\mathrm{clx}}$, $\boldsymbol{i}_{\mathrm{gx}}$ are all 3×1 column vectors, which represent the circulating current, upper arm voltage, lower arm voltage and the ac-side current in three-phase form. The subscript x represents the phase a, b, c. Since the ac-voltage control belongs to the fundamental frequency control, the modulation index can be linearized as:

$$\begin{cases}\Delta \boldsymbol{n}_{\mathrm{ux}}=-\dfrac{\Delta \boldsymbol{v}_{\mathrm{srefx}}}{V_{\mathrm{dc}}}\\ \Delta \boldsymbol{n}_{\mathrm{lx}}=\dfrac{\Delta \boldsymbol{v}_{\mathrm{srefx}}}{V_{\mathrm{dc}}}\end{cases} \tag{5}$$

2.2 Small-signal three-phase model of the ac-voltage loop

When applying the park and inverse park transform in the control part in d-q frame, the state variables in d-q form could be transformed into the three-phase form. The park and inverse park transform are listed in Appendix. The three-phase form of the inner current control loop is derived as.

$$\boldsymbol{v}_{\mathrm{srefx}}=\boldsymbol{T}^{\theta}_{dq/abc}\left(\boldsymbol{T}^{\theta}_{abc/dq}\left(K_{\mathrm{pi}}\left(\boldsymbol{i}_{\mathrm{grefx}}-\boldsymbol{i}_{\mathrm{ga}}\right)+K_{\mathrm{ii}}\boldsymbol{x}_{\mathrm{g1}x}\right)+\boldsymbol{T}^{\theta}_{abc/qd}K_{\mathrm{id}}\boldsymbol{i}_{gx}\right) \tag{6}$$

$$\begin{aligned}\frac{\mathrm{d}\boldsymbol{x}_{\mathrm{g1}x}}{\mathrm{dt}}&=\frac{\mathrm{d}}{\mathrm{dt}}\left(\boldsymbol{T}^{\theta}_{dq/abc}\boldsymbol{x}_{\mathrm{g1}dq}\right)=\omega_0\frac{\mathrm{d}\left(\boldsymbol{T}^{\theta}_{dq/abc}\right)}{\mathrm{d}\theta}\cdot\boldsymbol{x}_{\mathrm{g1}dq}+\boldsymbol{T}^{\theta}_{dq/abc}\frac{\mathrm{d}\boldsymbol{x}_{\mathrm{g1}dq}}{\mathrm{dt}}\\&=\omega_0\frac{\mathrm{d}}{\mathrm{d}\theta}\left(\boldsymbol{T}^{\theta}_{dq/abc}\right)\boldsymbol{T}^{\theta}_{abc/dq}\boldsymbol{x}_{\mathrm{g1}x}+\boldsymbol{T}^{\theta}_{dq/abc}\boldsymbol{T}^{\theta}_{abc/dq}\left(\boldsymbol{i}_{\mathrm{grefx}}-\boldsymbol{i}_{\mathrm{gx}}\right)\end{aligned} \tag{7}$$

Where the K_{pi}, K_{ii} is the gain of the proportional-integral regulator respectively, and the K_{id} represents the crossing-coupling term which equals to ωL. And the three-phase form of the outer voltage loop can be derived in the same way.

$$\boldsymbol{i}_{\mathrm{grefx}}=\boldsymbol{T}^{\theta}_{dq/abc}\left(\boldsymbol{T}^{\theta}_{abc/dq}\left(K_{\mathrm{pv}}\left(\boldsymbol{U}_{\mathrm{grefx}}-\boldsymbol{v}_{\mathrm{gx}}\right)-K_{\mathrm{f}}\boldsymbol{v}_{gx}+K_{\mathrm{iv}}\boldsymbol{x}_{\mathrm{g2}x}\right)\right) \tag{8}$$

$$\frac{\mathrm{d}\boldsymbol{x}_{\mathrm{g2}x}}{\mathrm{dt}}=\omega_0\frac{\mathrm{d}}{\mathrm{d}\theta}\left(\boldsymbol{T}^{\theta}_{abc/dq}\right)\cdot\boldsymbol{T}^{\theta}_{abc/dq}\boldsymbol{x}_{\mathrm{g2}x}+\boldsymbol{T}^{\theta}_{dq/abc}\cdot\boldsymbol{T}^{\theta}_{abc/dq}\left(\boldsymbol{U}_{\mathrm{grefx}}-\boldsymbol{v}_{\mathrm{gx}}\right) \tag{9}$$

Implementing the linearization on the equation from (6) to (9).

$$\Delta\boldsymbol{v}_{\mathrm{srefx}}=\boldsymbol{k}_1\left(K_{\mathrm{pi}}\left(\Delta\boldsymbol{i}_{\mathrm{grefx}}-\Delta\boldsymbol{i}_{\mathrm{ga}}\right)+K_{\mathrm{ii}}\Delta\boldsymbol{x}_{\mathrm{g1}x}\right)+\boldsymbol{k}_2K_{\mathrm{id}}\cdot\Delta\boldsymbol{i}_{\mathrm{ga}} \tag{10}$$

$$\frac{\mathrm{d}\Delta\boldsymbol{x}_{\mathrm{g1}x}}{\mathrm{dt}}=-\omega_0\boldsymbol{k}_2\cdot\Delta\boldsymbol{x}_{\mathrm{g1}x}+\boldsymbol{T}^{\theta}_{dq/abc}\boldsymbol{T}^{\theta}_{abc/dq}\left(\Delta\boldsymbol{i}_{\mathrm{grefx}}-\Delta\boldsymbol{i}_{\mathrm{gx}}\right) \tag{11}$$

$$\Delta\boldsymbol{i}_{\mathrm{grefx}}=\boldsymbol{T}^{\theta}_{dq/abc}\left(\boldsymbol{T}^{\theta}_{abc/dq}\left(-\left(K_{\mathrm{pv}}+K_{\mathrm{f}}\right)\cdot\Delta\boldsymbol{v}_{\mathrm{gx}}+K_{\mathrm{iv}}\cdot\Delta\boldsymbol{x}_{\mathrm{g2}x}\right)\right) \tag{12}$$

$$\frac{\mathrm{d}\Delta\boldsymbol{x}_{\mathrm{g2}x}}{\mathrm{dt}}=\omega_0\frac{\mathrm{d}}{\mathrm{d}\theta}\left(\boldsymbol{T}^{\theta}_{abc/dq}\right)\boldsymbol{T}^{\theta}_{abc/dq}\cdot\Delta\boldsymbol{x}_{\mathrm{g2}x}-\boldsymbol{T}^{\theta}_{dq/abc}\cdot\boldsymbol{T}^{\theta}_{abc/dq}\Delta\boldsymbol{v}_{\mathrm{gx}} \tag{13}$$

The multiplication term $\boldsymbol{k}_1$, $\boldsymbol{k}_2$ originated form the park and inverse park transform is constant which greatly simplifies the calculations. The value of the $\boldsymbol{k}_1$, $\boldsymbol{k}_2$ is listed in Appendix.

$$\boldsymbol{k}_1=\boldsymbol{T}^{\theta}_{dq/abc}\cdot\boldsymbol{T}^{\theta}_{abc/dq} \tag{14}$$

$$\boldsymbol{k}_2=\boldsymbol{T}^{\theta}_{dq/abc}\boldsymbol{T}^{\theta}_{abc/qd}=-\frac{\mathrm{d}}{\mathrm{d}\theta}\left(\boldsymbol{T}^{\theta}_{abc/dq}\right)\boldsymbol{T}^{\theta}_{abc/dq} \tag{15}$$

3 HSS-based Modified Sequence Impedance Model of MMC

3.1 HSS model of the MMC

In this part, the small-signal state-space model of the MMC derived in section 2 will be expanded in multi-harmonic domain based on the HSS. The procedure of transforming the time-domain state-space model into frequency-domain harmonic state-space model has been explained well in [11] and here the results are listed. The Toeplitz matrix $\boldsymbol{A}$ and $\boldsymbol{B}$ at each harmonic is shown in below.

$$\boldsymbol{A}=\begin{pmatrix} A_0 & A_{-1} & \cdots & A_{-h} & & & \\ A_1 & \ddots & \ddots & \ddots & \ddots & & \\ \vdots & \ddots & A_0 & A_{-1} & \ddots & \ddots & \\ A_h & \ddots & A_1 & A_0 & A_{-1} & \ddots & A_{-h} \\ & \ddots & \ddots & A_1 & A_0 & \ddots & \vdots \\ & & \ddots & \ddots & \ddots & \ddots & A_{-1} \\ & & & A_h & \cdots & A_1 & A_0 \end{pmatrix} \tag{16}$$

$$\boldsymbol{B}=\begin{pmatrix} B_0 & B_{-1} & \cdots & B_{-h} & & & \\ B_1 & \ddots & \ddots & \ddots & \ddots & & \\ \vdots & \ddots & B_0 & B_{-1} & \ddots & \ddots & \\ B_h & \ddots & B_1 & B_0 & B_{-1} & \ddots & B_{-h} \\ & \ddots & \ddots & B_1 & B_0 & \ddots & \vdots \\ & & \ddots & \ddots & \ddots & \ddots & B_{-1} \\ & & & B_h & \cdots & B_1 & B_0 \end{pmatrix} \tag{17}$$

According to the conclusion in [11], the accuracy of the HSS model can be guaranteed when the harmonic order h is set 4. The harmonic value (≤4) of each state variable can be calculated via the equation (20).

$$\boldsymbol{X}_p=-\left(\boldsymbol{A}-\boldsymbol{N}_p\right)^{-1}\boldsymbol{B}\cdot\boldsymbol{U}_p \tag{18}$$

Since the modulation signal is composed of only fundamental components, the matrix A higher than triple frequency can be set as zero matrix.

$$\boldsymbol{A}_{3\ldots h}=\boldsymbol{A}_{-3\ldots -h}=\boldsymbol{O}^{18\times 18} \tag{19}$$

The component of some symbols in (16) to (19) is shown below (h=4).

$$\boldsymbol{N}_p=\begin{bmatrix} j\left(\omega_p-4\omega_1\right)\boldsymbol{I}^{18\times 18} & & & & \\ & \ddots & & & \\ & & j\omega_p\boldsymbol{I}^{18\times 18} & & \\ & & & \ddots & \\ & & & & j\left(\omega_p+4\omega_1\right)\boldsymbol{I}^{18\times 18} \end{bmatrix} \tag{20}$$

$$\boldsymbol{X}_p=\begin{bmatrix} \boldsymbol{X}_{\left(\omega_p-4\omega_1\right)} \\ \vdots \\ \boldsymbol{X}_{\left(\omega_p-\omega_1\right)} \\ \boldsymbol{X}_{\left(\omega_p\right)} \\ \boldsymbol{X}_{\left(\omega_p+\omega_1\right)} \\ \vdots \\ \boldsymbol{X}_{\left(\omega_p+4\omega_1\right)} \end{bmatrix}_{162\times 1},\boldsymbol{X}_{\left(\omega_p\pm h\omega_1\right)}=\begin{bmatrix} \boldsymbol{I}_{cx\left(\omega_p\pm h\omega_1\right)} \\ \boldsymbol{V}^{\Sigma}_{cux\left(\omega_p\pm h\omega_1\right)} \\ \boldsymbol{V}^{\Sigma}_{clx\left(\omega_p\pm h\omega_1\right)} \\ \boldsymbol{I}_{gx\left(\omega_p\pm h\omega_1\right)} \\ \boldsymbol{X}_{g1x\left(\omega_p\pm h\omega_1\right)} \\ \boldsymbol{X}_{g2x\left(\omega_p\pm h\omega_1\right)} \end{bmatrix}_{18\times 1} \tag{21}$$

Here, the positive sequence voltage disturbance is selected as an injection example.

$$\boldsymbol{U}_p=\begin{bmatrix} \boldsymbol{U}_{\left(\omega_p-4\omega_1\right)} \\ \vdots \\ \boldsymbol{U}_{\left(\omega_p-\omega_1\right)} \\ \boldsymbol{U}_{\left(\omega_p\right)} \\ \boldsymbol{U}_{\left(\omega_p+\omega_1\right)} \\ \vdots \\ \boldsymbol{U}_{\left(\omega_p+4\omega_1\right)} \end{bmatrix},\boldsymbol{U}_{\left(\omega_p\right)}=\begin{bmatrix} \boldsymbol{0}_{3\times 1} \\ \boldsymbol{0}_{3\times 1} \\ \boldsymbol{0}_{3\times 1} \\ V_p \\ V_p e^{-j\frac{2\pi}{3}} \\ V_p e^{j\frac{2\pi}{3}} \\ \boldsymbol{0}_{3\times 1} \\ \boldsymbol{0}_{3\times 1} \end{bmatrix},\boldsymbol{U}_{\left(\omega_p\pm h\omega_1\right)}=\boldsymbol{O}^{18\times 1} \tag{22}$$

3.2 Modified sequence impedance model of the MMC

In this part, the linear symmetric transform is applied in the three-phase state variables to acquire the sequence components. The symmetric transform is extended as.

$$\boldsymbol{E}=\begin{bmatrix} \boldsymbol{e} & & & & & \\ & \boldsymbol{e} & & & & \\ & & \boldsymbol{e} & & & \\ & & & \boldsymbol{e} & & \\ & & & & \boldsymbol{e} & \\ & & & & & \boldsymbol{e} \end{bmatrix}_{12\times 18},\boldsymbol{e}=\frac{1}{3}\begin{bmatrix} 1 & e^{j\frac{2\pi}{3}} & e^{-j\frac{2\pi}{3}} \\ 1 & e^{-j\frac{2\pi}{3}} & e^{j\frac{2\pi}{3}} \end{bmatrix}_{2\times 3} \tag{23}$$

By applying the extended symmetric transform, the sequence component of the ac-side voltage and current can be gotten as.

$$\boldsymbol{I}_{gpn}=\boldsymbol{E}\begin{bmatrix} \boldsymbol{I}_{gx\left(\omega_p-4\omega_1\right)} \\ \vdots \\ \boldsymbol{I}_{gx\left(\omega_p-\omega_1\right)} \\ \boldsymbol{I}_{gx\left(\omega_p\right)} \\ \boldsymbol{I}_{gx\left(\omega_p+\omega_1\right)} \\ \vdots \\ \boldsymbol{I}_{gx\left(\omega_p+4\omega_1\right)} \end{bmatrix},\boldsymbol{V}_{gpn}=\boldsymbol{E}\left(\begin{bmatrix} \boldsymbol{I}_{gx\left(\omega_p-4\omega_1\right)} \\ \vdots \\ \boldsymbol{I}_{gx\left(\omega_p-\omega_1\right)} \\ \boldsymbol{I}_{gx\left(\omega_p\right)} \\ \boldsymbol{I}_{gx\left(\omega_p+\omega_1\right)} \\ \vdots \\ \boldsymbol{I}_{gx\left(\omega_p+4\omega_1\right)} \end{bmatrix}Z_L+\begin{bmatrix} \boldsymbol{0}_{3\times 1} \\ \vdots \\ \boldsymbol{0}_{3\times 1} \\ \boldsymbol{V}_{px} \\ \boldsymbol{0}_{3\times 1} \\ \vdots \\ \boldsymbol{0}_{3\times 1} \end{bmatrix}\right) \tag{24}$$

As stated in [8], the modified sequence matrix needs two independent injections to be calculated, for example, positive sequence injection and negative sequence injection.

$$\begin{bmatrix} Z_{pp} & Z_{pn} \\ Z_{np} & Z_{nn} \end{bmatrix} = \begin{bmatrix} V_{p1} & V_{p2} \\ V_{n1} & V_{n2} \end{bmatrix} \begin{bmatrix} I_{p1} & I_{p2} \\ I_{n1} & I_{n2} \end{bmatrix}^{-1} \tag{25}$$

For the positive sequence voltage disturbance injection ($\boldsymbol{V}_{px}$=[V_{p} $V_{\mathrm{p}}e^{-j2\pi/3}$ $V_{\mathrm{p}}e^{j2\pi/3}$]^T), the corresponding extracted ac-side voltage and current in sequence form is shown.

$$\begin{aligned} V_{p1} &= V_{gpn}^{\mathrm{P}}(\omega_p), & I_{p1} &= I_{gpn}^{\mathrm{P}}(\omega_p), \\ V_{n1} &= V_{gpn}^{\mathrm{N}}(\omega_p - 2\omega_1), & I_{n1} &= I_{gpn}^{\mathrm{N}}(\omega_p - 2\omega_1) \end{aligned} \tag{26}$$

For the negative sequence voltage disturbance injection ($\boldsymbol{V}_{px}$=[V_{p} $V_{\mathrm{p}}e^{j2\pi/3}$ $V_{\mathrm{p}}e^{-j2\pi/3}$]^T), the corresponding extracted ac-side voltage and current in sequence form is shown.

$$\begin{aligned} V_{n2} &= V_{gpn}^{\mathrm{N}}(\omega_n), & I_{n2} &= I_{gpn}^{\mathrm{N}}(\omega_n) \\ V_{p2} &= V_{gpn}^{\mathrm{P}}(\omega_n + 2\omega_1), & I_{p2} &= I_{gpn}^{\mathrm{P}}(\omega_n + 2\omega_1) \end{aligned} \tag{27}$$

4 The stability analysis of the interconnected system

The parameters of the studied interconnected system are listed in Table 1. In this part, the correctness of the derived MIMO impedance model of the MMC under ac-voltage control is verified via the frequency scanning method.

Table 1 Main Parameters of the interconnected system

	Description	Value
MMC	Arm resistance	1 Ω
	Arm inductance	360 mH
	Sub-module capacitance	140 μF
	Number of arm sub-modules	20
	Dc-link Voltage	320 kV
	Grid frequency	50 Hz
Wind turbine	Power rating	2MW
	Dc bus voltage	1100V
	Dc bus capacitor	35 mF
	filter inductance	0.15 mH

As shown in Fig.2, the analytical impedance curves are consistent with frequency scanning impedance curves both in diagonal and off-diagonal components, including magnitude and phase curves. It can be observed that the off-diagonal component is relatively high especially in middle and low frequency range (1 ~ 250Hz).

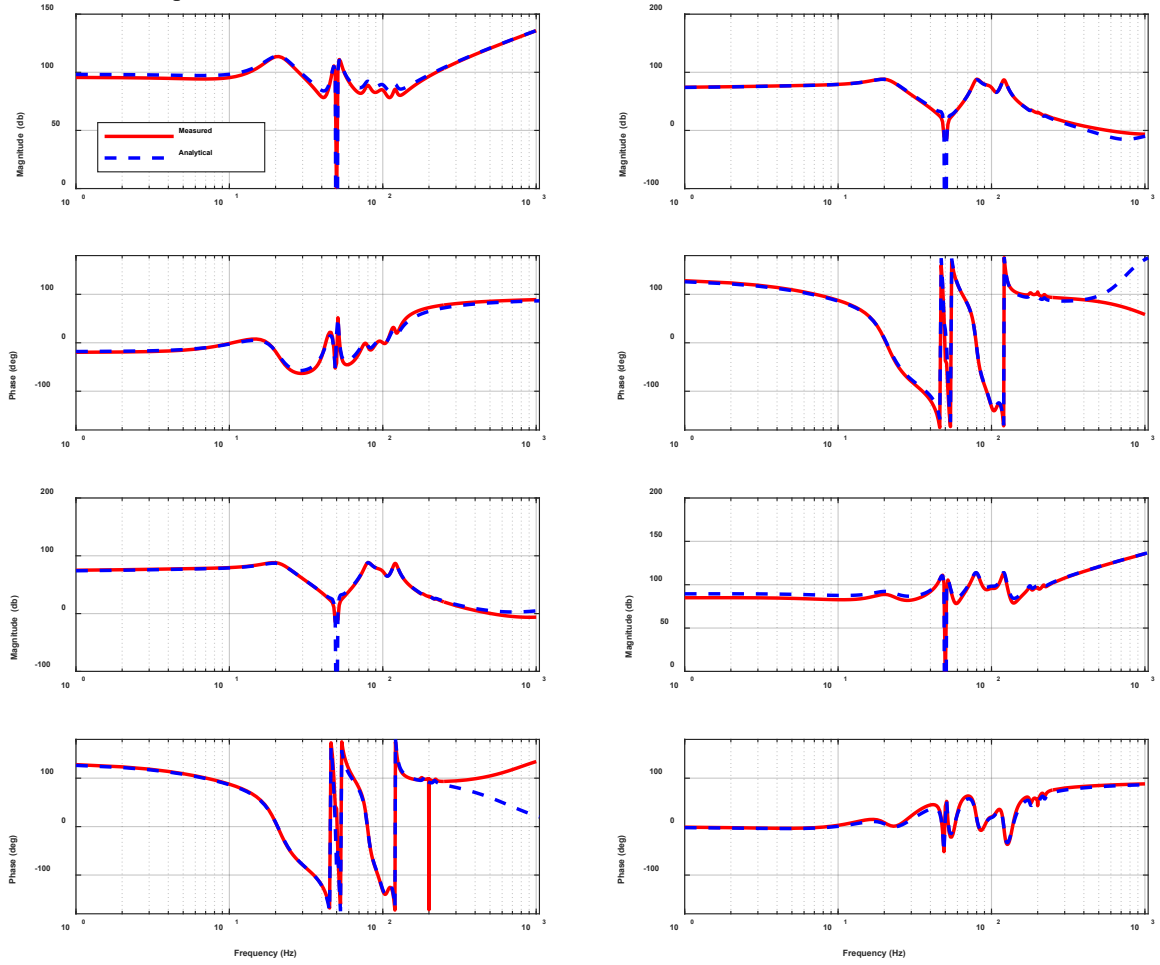

Fig. 2 Verification of the MIMO impedance model of the MMC

The MIMO impedance model in [13] is used in this paper which is detailed and takes into account of the dc dynamics. The wind farm is aggregated according to the method in [15], [16]. When the output power of the wind farm increase, the stability margin of the interconnected system declines continuously. As shown in Fig.3, when the number of the wind turbine within the wind farm reaches 4, the system nearly reaches the critical state. When the number of the wind turbine is 5, the system becomes unstable. The results of the theoretical analysis are verified by time domain simulation as shown in Fig.4. Through the FFT analysis shown in Fig.5, the oscillation frequency is 20Hz which is in line with the theoretical analysis. Actually, due to that there is no circulating current suppressing control, the oscillation is mainly caused by the double-frequency component around the 20Hz.

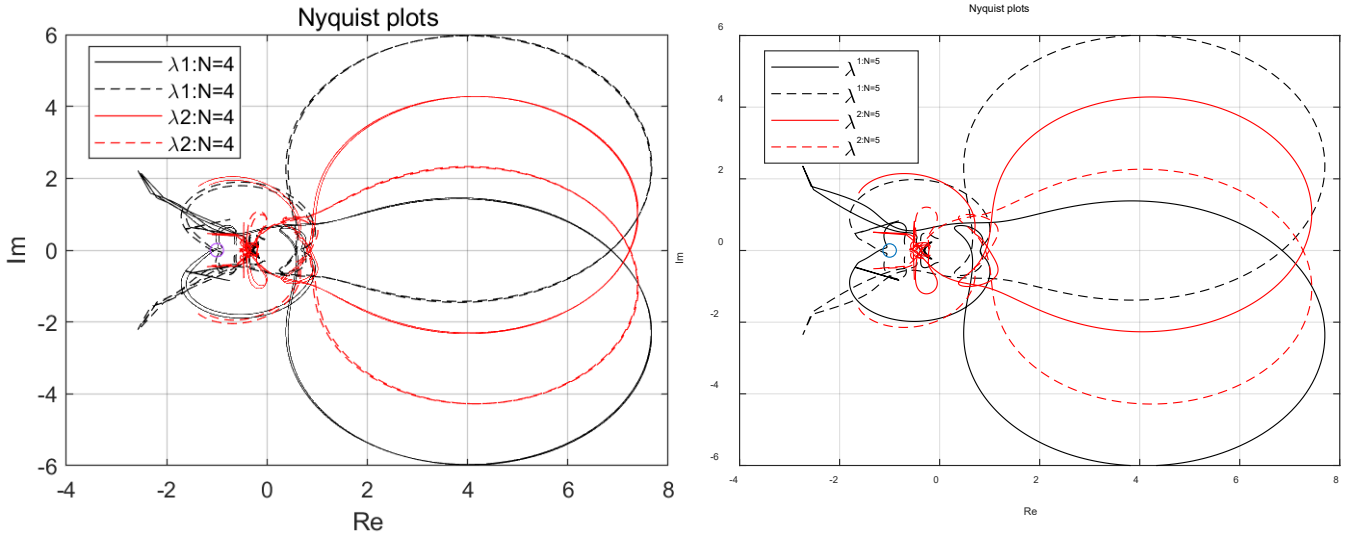

Fig. 3 Theoretical analysis of the interconnected system

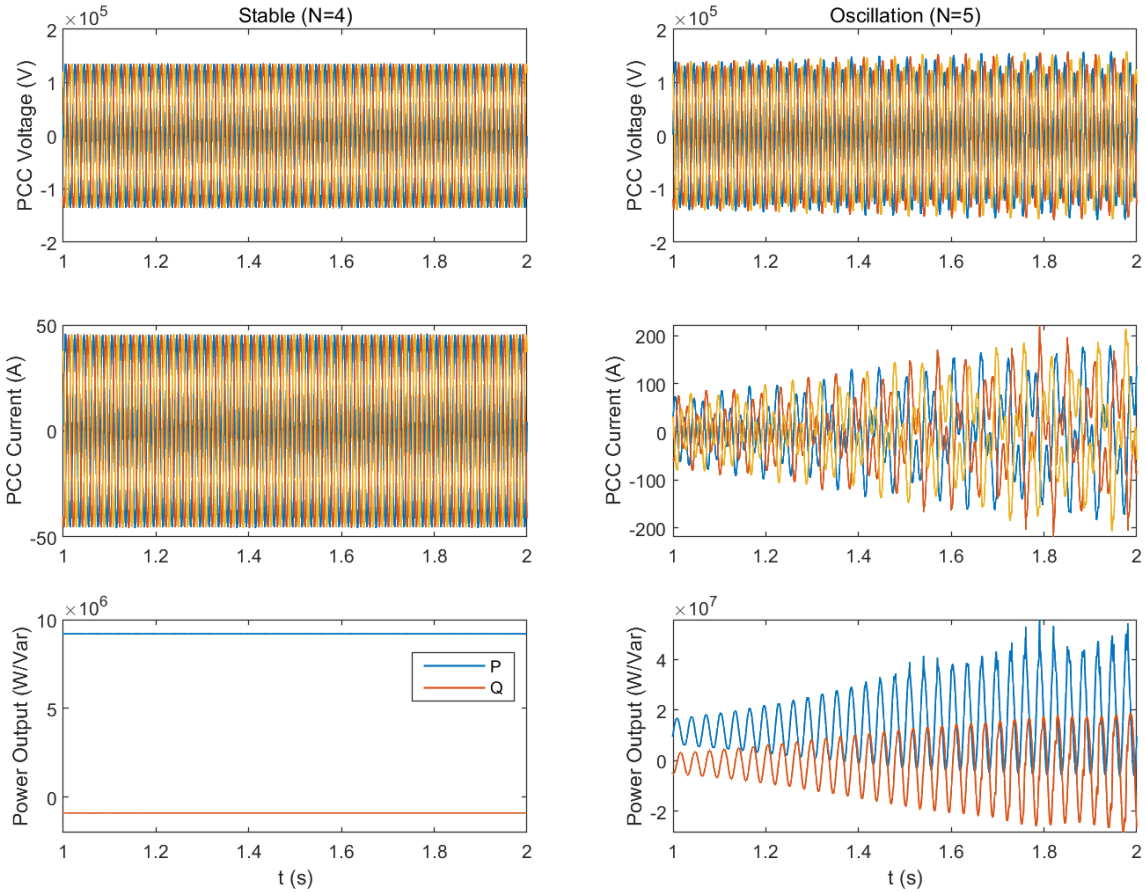

Fig. 4 Time-domain simulation verifications.

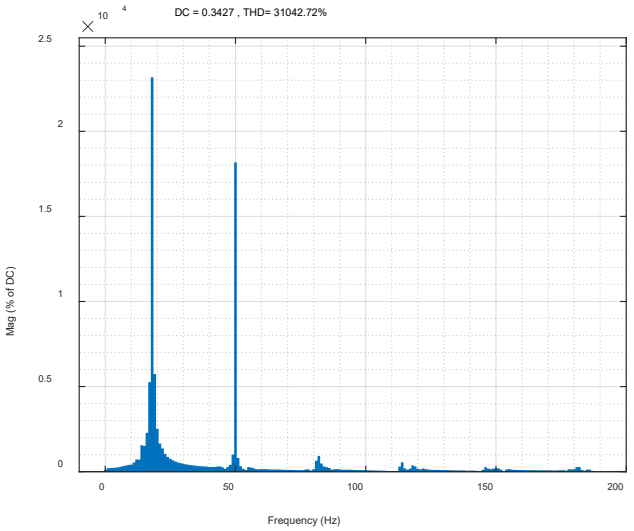

Fig. 5 FFT analysis of the unstable ac-side current (N=5)

5 Conclusion

This work mainly presents the stability analysis of the wind farm system connected with the MMC-HVDC in modified sequence domain. The MIMO modified sequence impedance model of the MMC under ac-voltage control is developed in this paper which fits well with the frequency scanning results. Despite that the detailed wind turbine model is used in this paper, the aggregation model of the wind farm is still applied for simplicity. In the future work, the detailed wind farm model will be used for interaction analysis. The effects of the off-diagonal couplings both from the MMC and the wind farm will be analyzed.

6 Acknowledgements

This work was supported by the National Natural Science Foundation of China under Grant 51837007. The authors would like to thank team members at SJTU, and co-workers from NTNU for their valuable advices.

7 References

[1] Debnath, S., Qin, J., Bahrani, B., et al.: 'Operation, Control, and Applications of the Modular Multilevel Converter: A Review', IEEE Transactions on Power Electronics., 2015, 30, (1), pp. 37-53

[2] Lyu, J., Cai, X., Molinas, M.: 'Frequency domain stability analysis of MMC-based HVdc for wind farm integration', IEEE Journal of Emerging and Selected Topics in Power Electronics., 2016, 4, (1), pp. 141-151

[3] Lyu, J., Cai, X., Amin, M., Molinas, M.: 'Subsynchronous oscillation mechanism and its suppression in MMC-Based HVDC connected wind farms', IET Generation, Transmission & Distribution., 2018, 12, (4), pp. 1021-1029

[4] Zong, H., Lyu, J., Cai, X., M., Molinas, et al.: 'Analysis of Bifurcation Behaviors in MMC Connected to a Weak Grid, ' IECON 2018 - 44th Annual Conference of the IEEE Industrial Electronics Society, Washington, DC, 2018, pp. 1687-1692

[5] Lyu, J., Cai, X., Molinas, M.: 'Optimal design of controller parameters for improving the stability of MMC-HVDC for wind farm integration', IEEE Journal of Emerging and Selected Topics in Power Electronics, 2018, 6, (1), pp. 40-53

[6] Amin, M., Ardal, A., Molinas, M.: 'Self-synchronisation of wind farm in MMC-based HVDC system: a stability investigation', IEEE Trans. Energy Convers., 2017, 32, (2), pp. 458–470

[7] Zhu, M., Nian, H., Xu, Y., et al.: 'Impedance-Based Stability Analysis of MMC-HVDC for Offshore DFIG-Based Wind Farms', Proc. ICEMS, Jeju, South Korea, Oct. 2018, pp. 1139–1144

[8] Rygg, A., Molinas, M., Zhang, C. and Cai, X.: 'A Modified Sequence-Domain Impedance Definition and Its Equivalence to the dq-Domain Impedance Definition for the Stability Analysis of AC Power Electronic Systems', IEEE Journal of Emerging and Selected Topics in Power Electronics., 2016, 4, (4), pp. 1383-1396

[9] Sun, J. and Liu, H.: 'Sequence Impedance Modeling of Modular Multilevel Converters', IEEE Journal of Emerging and Selected Topics in Power Electronics., 2017, 5, (4), pp. 1427-1443

[10] Sun, J. and Liu, H.: 'Impedance modeling and analysis of modular multilevel converters', 2016 IEEE 17th Workshop on Control and Modeling for Power Electronics (COMPEL), Trondheim., 2016, pp. 1-9

[11] Lyu, J., Zhang, X., Cai, X., and Molinas, M.: 'Harmonic state-space based small-signal impedance modeling of modular multilevel converter with consideration of internal harmonic dynamics', IEEE Transactions on Power Electronics., 2019, 34, (3), pp. 2134-2148

[12] Chen, Q., Lyu, J., Li, R., et al.: 'Impedance modeling of modular multilevel converter based on harmonic state space, ' 2016 IEEE 17th Workshop on Control and Modeling for Power Electronics (COMPEL), Trondheim, 2016, pp. 1-5

[13] Zhang, C., Cai, X., Molinas, M. and Rygg, A.: 'Frequency-domain modelling and stability analysis of a DFIG-based wind energy conversion system under non-compensated AC grids: impedance modelling effects and consequences on stability', IET Power Electronics., 2019, 12, (4), pp. 907-914

[14] Gilbert, Bergna., Suul, J. A., and D'Arco, S.: 'State-space modelling of modular multilevel converters for constant variables in steady-state', 2016 IEEE 17th Workshop on Control and Modeling for Power Electronics (COMPEL), Trondheim, 2016, pp. 1-9.

[15] Zong, H., Lyu, J., Cai, X., et al.: 'Accurate Aggregated Modelling of Wind Farm Systems in Modified Sequence Domain for Stability Analysis', Electric Power Systems Research, 2019, to be published

[16] Zhang, C., Molinas, M., Rygg, A. and Cai, X.: 'Impedance-based Analysis of Interconnected Power Electronics Systems: Impedance Network Modeling and Comparative Studies of Stability Criteria', 2019, IEEE Journal of Emerging and Selected Topics in Power Electronics, early access.

8 Appendix

Park and inverse park transform are shown below.

$$\boldsymbol{T}_{abc/dq}^{\theta}=\frac{2}{3}\cdot\begin{bmatrix}\cos\theta & \cos\left(\theta-\frac{2}{3}\pi\right) & \cos\left(\theta+\frac{2}{3}\pi\right)\\ -\sin\theta & -\sin\left(\theta-\frac{2}{3}\pi\right) & -\sin\left(\theta+\frac{2}{3}\pi\right)\end{bmatrix} \quad \text{(A1)}$$

$$\boldsymbol{T}_{dq/abc}^{\theta}=\begin{bmatrix}\cos\theta & \cos\left(\theta-\frac{2}{3}\pi\right) & \cos\left(\theta+\frac{2}{3}\pi\right)\\ -\sin\theta & -\sin\left(\theta-\frac{2}{3}\pi\right) & -\sin\left(\theta+\frac{2}{3}\pi\right)\end{bmatrix}^{T} \quad \text{(A2)}$$

$$\boldsymbol{T}_{abc/qd}^{\theta}=\frac{2}{3}\cdot\begin{bmatrix}\sin\theta & \sin\left(\theta-\frac{2}{3}\pi\right) & \sin\left(\theta+\frac{2}{3}\pi\right)\\ \cos\theta & \cos\left(\theta-\frac{2}{3}\pi\right) & \cos\left(\theta+\frac{2}{3}\pi\right)\end{bmatrix} \quad \text{(A3)}$$

The $\boldsymbol{T}_{cos}$ and $\boldsymbol{T}_{sin}$ is used to represent the first and second row of the (A1) respectively.
The concrete value of the $\boldsymbol{k_1}$ and $\boldsymbol{k_2}$ is listed here.

$$\boldsymbol{k}_1=\frac{2}{3}\cdot\begin{bmatrix}1 & -\frac{1}{2} & -\frac{1}{2}\\ -\frac{1}{2} & 1 & -\frac{1}{2}\\ -\frac{1}{2} & -\frac{1}{2} & 1\end{bmatrix} \quad \text{(A4)}$$

$$\boldsymbol{k}_2=\frac{2}{3}\cdot\begin{bmatrix}0 & -\frac{\sqrt{3}}{2} & \frac{\sqrt{3}}{2}\\ \frac{\sqrt{3}}{2} & 0 & -\frac{\sqrt{3}}{2}\\ -\frac{\sqrt{3}}{2} & \frac{\sqrt{3}}{2} & 0\end{bmatrix} \quad \text{(A5)}$$